JVSTB
Journal of Vacuum Science & Technology B

Silicon photodetectors integrated with vertical silicon nitride waveguides as image sensor pixels: Fabrication and characterization

Turgut Tut, Yaping Dan, Peter Duane, Winnie N. Ye, Fatih Degirmenci, Young Yu, Munib Wober, and Kenneth B. Crozier

Citation: Journal of Vacuum Science & Technology B **32**, 031201 (2014); doi: 10.1116/1.4868627
View online: http://dx.doi.org/10.1116/1.4868627
View Table of Contents: http://scitation.aip.org/content/avs/journal/jvstb/32/3?ver=pdfcov
Published by the AVS: Science & Technology of Materials, Interfaces, and Processing

---

Articles you may be interested in
Dielectric waveguide vertically coupled to all-silicon photodiodes operating at telecommunication wavelengths
Appl. Phys. Lett. **102**, 171106 (2013); 10.1063/1.4803541

Efficient and broadband polarization rotator using horizontal slot waveguide for silicon photonics
Appl. Phys. Lett. **101**, 021105 (2012); 10.1063/1.4734640

Vertical waveguides integrated with silicon photodetectors: Towards high efficiency and low cross-talk image sensors
Appl. Phys. Lett. **100**, 043504 (2012); 10.1063/1.3678019

Near-infrared waveguide-based nickel silicide Schottky-barrier photodetector for optical communications
Appl. Phys. Lett. **92**, 081103 (2008); 10.1063/1.2885089

Subterranean silicon photonics: Demonstration of buried waveguide-coupled microresonators
Appl. Phys. Lett. **87**, 081114 (2005); 10.1063/1.2009062

AVS
Re-register for Table of Content Alerts
Create a profile.
Sign up today!

Redistribution subject to AVS license or copyright; see http://scitation.aip.org/termsconditions. Download to IP: 202.120.43.250 On: Mon, 05 May 2014 11:30:58

Silicon photodetectors integrated with vertical silicon nitride waveguides as image sensor pixels: Fabrication and characterization

Turgut Tut[a)]
School of Engineering and Applied Sciences, Harvard University, 33 Oxford Street, Cambridge, Massachusetts 02138 and TUBİTAK MAM ME, Gebze 41470, Turkey

Yaping Dan
School of Engineering and Applied Sciences, Harvard University, 33 Oxford Street, Cambridge, Massachusetts 02138

Peter Duane
School of Engineering and Applied Sciences, Harvard University, 33 Oxford Street, Cambridge, Massachusetts 02138 and Zena Technologies Inc., 174 Haverhill Road, Topsfield, Massachusetts 01983

Winnie N. Ye
School of Engineering and Applied Sciences, Harvard University, 33 Oxford Street, Cambridge, Massachusetts 02138

Fatih Degirmenci
School of Engineering and Applied Sciences, Harvard University, 33 Oxford Street, Cambridge, Massachusetts 02138 and TUBİTAK MAM ME, Gebze 41470, Turkey

Young Yu
Zena Technologies Inc., 174 Haverhill Road, Topsfield, Massachusetts 01983

Munib Wober
School of Engineering and Applied Sciences, Harvard University, 33 Oxford Street, Cambridge, Massachusetts 02138 and Zena Technologies Inc., 174 Haverhill Road, Topsfield, Massachusetts 01983

Kenneth B. Crozier
School of Engineering and Applied Sciences, Harvard University, 33 Oxford Street, Cambridge, Massachusetts 02138

(Received 9 December 2013; accepted 3 March 2014; published 17 March 2014)

The current trend toward image sensors with ever-increasing pixel counts is prompting continual reductions in pixel area, leading to significant cross-talk and efficiency challenges. The realization of image sensor pixels containing waveguides presents a means for addressing these issues. The fabrication of such pixels is however not straightforward. Conventional waveguides employed in integrated optics are horizontal, but waveguides needed for the proposed sensor must be vertical and integrated with photodetectors. Here, the authors describe a fabrication process for vertical silicon nitride waveguides integrated with silicon photodetectors. The authors describe the etching, deposition, and planarization techniques that enable the formation of silicon nitride waveguides embedded in silicon dioxide. They also describe a fabrication process for silicon photodetectors, including a means for ensuring that their photosensitive areas have sizes consistent with those of photodetectors employed in conventional image sensors. In addition, the authors perform optical and electrical characterization of the fabricated devices. The results demonstrate the ability of the fabricated waveguides to guide light onto the photodetectors with high efficiency. *© 2014 American Vacuum Society*. [http://dx.doi.org/10.1116/1.4868627]

I. INTRODUCTION

In recent years, there has been enormous growth in the prevalence of digital imaging systems in consumer applications. The image sensors used in these systems are being increasingly dominated by complementary metal oxide semiconductor (CMOS) technology. For many applications, there has been a market demand for increased spatial resolution. This has been largely achieved by decreasing the pixel size, which has reduced from more than 10 μm to less than 2 μm over approximately one decade.[1] It has been predicted that optical efficiency will be reduced and interpixel cross-talk increased as conventional image sensor pixels are scaled to submicron dimensions.[1] As we discuss further below, vertical waveguides, or "light pipes," present a means for overcoming these fundamental challenges. Fesenmeier *et al.* simulated light pipe structures.[2] Hsu *et al.*[3] and Gambino *et al.*[4] demonstrated light pipe devices experimentally, with pipe heights ranging from 2.2 to 4 μm, by stacking multiple etched sections. We previously demonstrated the ability of silicon nitride light pipes to improve optical efficiency.[5] Here, we describe the fabrication processes that enables the formation of silicon nitride light pipes integrated with photodetectors. These are described in a level of detail not present in Ref. 5. We demonstrate the deposition of silicon nitride with good optical properties and the etching process to form pillars. We

---

[a)] Electronic mail: turgut.tut@tubitak.gov.tr

Redistribution subject to AVS license or copyright; see http://scitation.aip.org/termsconditions. Download to IP: 202.120.43.250 On: Mon, 05 May 2014 11:30:58

also present a process for encasing the pillars in silicon dioxide by deposition and chemical mechanical polishing (CMP). The integration of the light pipes formed in this way with silicon photodetectors is discussed. We demonstrate a means for ensuring that the photosensitive regions of these photodetectors have sizes comparable to those of traditional image sensor pixels. As discussed below, this is critical in order for optical performance enhancement enabled by our light pipes to be demonstrated. The current–voltage characteristics of the completed devices under dark and illuminated conditions are presented. Finally, we present results confirming that the light pipes guide light onto the photodetectors with high efficiency.

The ability of light pipes to improve optical performance in scaled image sensor pixels arises from both geometric optics and diffraction effects. We begin by considering geometric optics effects. Light incident on a conventional image sensor pixel is focused by a microlens through the dielectric stack onto a photodetector. Reducing the pixel size while maintaining the microlens-to-photodetector distance leads to increased interpixel cross talk and lower optical efficiency, especially for light incident at other than normal incidence. This can be understood from Fig. 1. A conventional image sensor pixel is shown as Fig. 1(a). Light at normal incidence is focused to the photodetector center. A consequence of the finite size of the photodetector (diameter R), however, is that only light incident on the microlens up to a maximum angle of ϕ_I can be collected onto the photodetector. This angle is given approximately by $\phi_1 \approx nR/(2F_1)$. Here, n is the microlens refractive index (assumed to be equal to that of the dielectric stack) and F_1 is its focal length. As pixel dimensions (and therefore R) shrink, and the microlens-to-photodetector distance (and hence F) is maintained or increased, the maximum acceptance angle (ϕ_1) decreases, leading to efficiency and interpixel cross-talk issues. In Fig. 1(b), it can be seen that the light pipe increases the acceptance angle (to $\phi_2 \approx nR/(2F_2)$), due to the fact that the microlens has a shorter focal length (F_2). These geometric optics considerations therefore predict that light pipes enhance the optical performance. They also emphasize if a device is built to demonstrate the improved performance possible with light pipes, then the photodetector will need to have a photosensitive region (diameter R) that is limited in extent (and consistent with the dimensions of photodetectors in actual image sensors) for the enhancement to be confirmed. It has also been noted that diffraction effects become very pronounced for submicron pixels,[1] a consequence of the fact that the microlens has an extent of only a few wavelengths, which prohibits efficient focusing of the incident light on the photodetector.[1] Here, light pipes present a means for improving optical performance as the light only needs to be focused onto the light pipe's entrance, rather than through the full dielectric stack onto the photodetector. The use of the light pipe is therefore akin to reducing the stack height. Simulations have predicted that stack height reduction should enable submicron pixels to achieve good optical performance.[1]

The organization of this paper is as follows. We describe the fabrication of the silicon nitride light pipes and silicon photodetectors in Secs. II A and II B, respectively. For the latter, we include a discussion of the fabrication steps that enable the successful integration of light pipes and photodetectors. In Sec. III, optical and electrical measurements are presented to demonstrate that the device achieves the desired efficiency improvement. Conclusions are presented in Sec. IV.

II. FABRICATION RESULTS

A. Fabrication of silicon nitride light pipes

One approach to the realization of silicon nitride light pipes embedded in silicon dioxide involves the following steps. Silicon dioxide is first deposited, for example by plasma-enhanced chemical vapor deposition (PECVD). Holes are then produced by standard optical lithography and reactive ion etching. The holes are then filled by the deposition of silicon nitride by PECVD. We have previously demonstrated this approach[6] with challenges. While silicon nitride generally deposits much more conformally by PECVD than by low pressure chemical vapor deposition, it is however not close to being ideal. Deposition rates are higher at the trench corners than those along the trench sides. As a result, the top openings of the holes close, preventing further filling, leading to void formation (Fig. 2). We therefore develop an alternative method

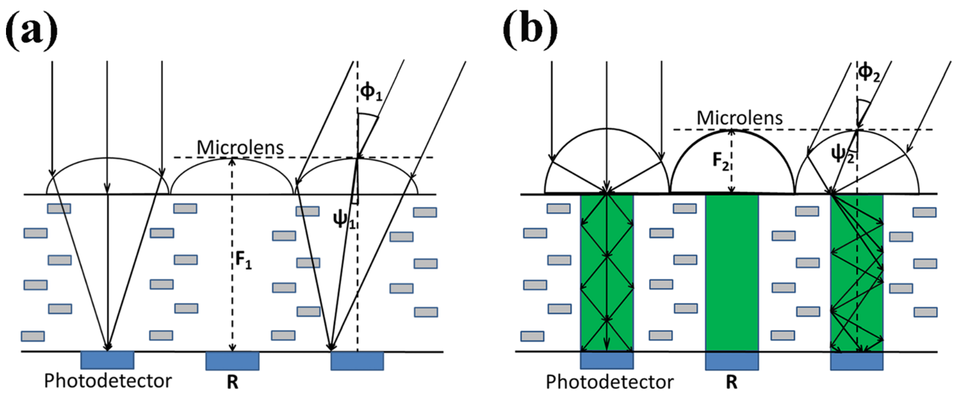

FIG. 1. (Color online) (a) On the left, a typical image sensor pixel where microlens focuses incident light on the center of the photodetector. On the right, Φ_1 is the maximum incident angle of light that photodetector can detect (b) On the left, an image sensor pixel with light-pipe (waveguide situated between color filter and photodetector) where light is focused by microlens on top of the light-pipe and guided through the photodetector. On the right, Φ_2 is the maximum incident angle of light that can be focused by microlens on top of the light-pipe and detected by the photodetector at the bottom.

Redistribution subject to AVS license or copyright; see http://scitation.aip.org/termsconditions. Download to IP: 202.120.43.250 On: Mon, 05 May 2014 11:30:58

in which the silicon nitride is etched to form pillars, followed by being encased in silicon dioxide. The first step of this process involves the deposition of silicon nitride by PECVD. For the proposed application, it is of course important that the silicon nitride exhibits good optical transmission. The PECVD-grown SiN_x film under study has acceptable optical transmission in 400–900 nm spectral range. Figure 3(a) shows the transmission spectra of 9 μm thick films of SiN_x and SiO_2. It can be seen that SiN_x film deposited with a flow rate of 35 sccm SiH_4 has far higher optical transmission than that deposited at 40 sccm, which is consistent with previous studies.[7,8] In the light pipe devices described in the remainder of this paper, the deposition of SiN_x follows the process parameters with the flow rates of SiH_4, NH_3, and N_2 being set to 35, 40, and 1960 sccm, respectively. The radiofrequency (RF) powers at high and low frequencies are 21 W and 50 W, respectively. The platen and lid temperatures are 300 °C and 250 °C, respectively. The chamber pressure is 900 mTorr. This results in an SiN_x deposition rate of 11.6 nm/min. A deposition rate of 18.75 nm/min results when the SiH_4 flow rate is increased to 40 sccm, while keeping all other parameters the same.

We now describe the fabrication of silicon nitride pillars. We first deposit SiN_x to a thickness of 8 μm using the method described above. We then perform optical lithography, thermally evaporate a layer of Al (50 nm) and perform the lift off process. This yields an array of Al disks (5 μm diameter) that serve as etch masks. We consider the etching step we perform next to be the most challenging part of the fabrication process. Inductively coupled plasma reactive ion etching [ICP-RIE, surface technology systems (STS)] is used with an SF_6/C_4F_8 gas mixture. The SF_6 gas is responsible for the etching, and acts in an isotropic fashion. The C_4F_8 gas is responsible for the formation of a polymer layer, and therefore promotes anisotropic etching. We find that it also enhances the smoothness of the sidewalls and of the bottom surface but decreases the etch rate. The etch rate depends on the diameter of the pillars, the distance between the pillars, the ratio of the flow rates of the gases and the pressure in the chamber, the coil, and RF powers. In this work, we experiment with varying the ratio between the flow rates of the etching gases C_4F_8 and SF_6, with the aim of achieving silicon nitride pillars with vertical side walls. The C_4F_8 flow rate is maintained at 150 sccm for C_4F_8/SF_6 gas flow ratios greater than 1.0, while the SF_6 flow rate is maintained at 130 sccm for C_4F_8/SF_6 ratios below 1.0. We find that vertical light pipes, with sidewall angles close to 90°, are achieved at relatively high C_4F_8 to SF_6 flow rate ratios [Fig. 3(b)]. The etch rate is reduced at such ratios, but sufficiently high for the light pipes to be produced in a reasonable time. We note however that polymer forms during the etch process, which may lead to micromasking and increased surface roughness. We address this problem by two methods that use O_2 gas. In one approach, a small amount of O_2 (4 sccm flow rate) is added to the C_4F_8/SF_6 etch process. This helps remove polymer that forms on the sidewalls. The second method comprises the use of an O_2 plasma for 30 min after the formation of the light pipes. The use of O_2 to mitigate the polymer formation is described further below.

We find that the silicon nitride pillars are etched with undercutting of the Al disk masks. The desired final pillar diameter can be achieved by increasing the diameter of the etch mask for the Al disk. Figure 4(a) shows a silicon nitride pillar produced by etching for 2 hours (C_4F_8 flow rate: 150 sccm, SF_6 flow rate: 75 sccm, coil power: 1200 W, platen

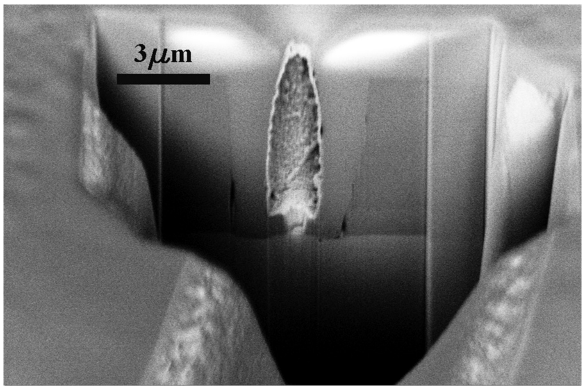

FIG. 2. Scanning electron micrograph of structure resulting when SiN_x is deposited into a cylindrical hole opened in a thick SiO_2 layer. It can be seen that the nonconformal deposition of SiN_x results in the formation of a keyhole, i.e., incomplete filling.

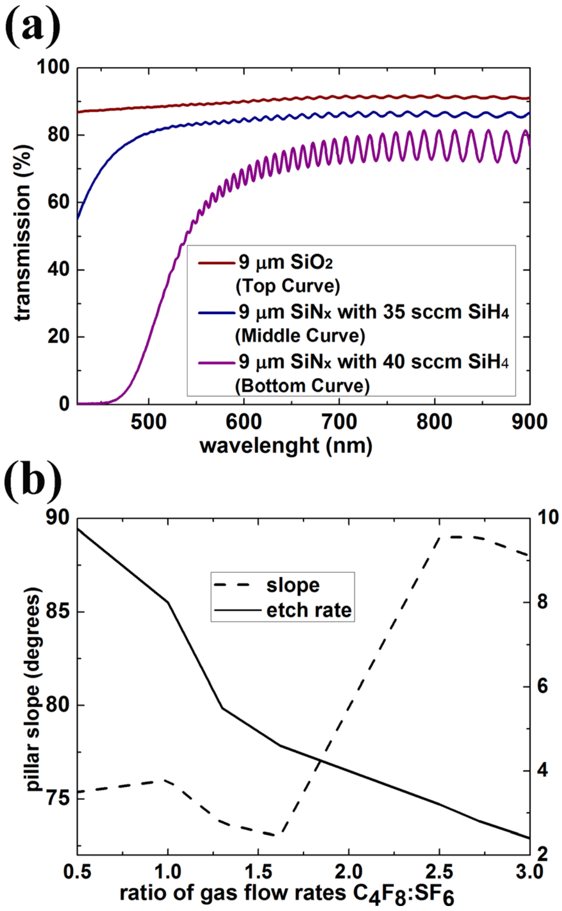

FIG. 3. (Color online) (a) Measured optical transmission spectra of the thin films used in light pipe fabrication. (b) Solid curve: Dependence of SiN_x etch rate upon ratio between C_4F_8 and SF_6 gases. Dotted curve: dependence of slope of light pipe walls with etch gas ratio.

Redistribution subject to AVS license or copyright; see http://scitation.aip.org/termsconditions. Download to IP: 202.120.43.250 On: Mon, 05 May 2014 11:30:58

power: 12 W, pressure: 10 mTorr, and temperature: 25 °C). The pillar is 8.5 μm tall and has a diameter of 4 μm. The diameters of the disks of the photomask are 5 μm. Polymer produced during the etch process can be seen near the bottom of the lower light pipe of Fig. 4(a). In order to remove the undesirable polymer, we add O_2 gas (flow rate 4 sccm) to the SF_6/C_4F_8 ICP RIE process, and increase the pressure to 15 mTorr. Other parameters remain the same (C_4F_8 flow rate: 150 sccm, SF_6 flow rate: 75 sccm, coil power: 1200 W, and platen power: 12 W). The SiN_x deposited with an SiH_4 flow rate of 35 sccm is found to be smoother than that deposited with a SiH_4 flow rate of 40 sccm, possibly due to the lower deposition rate (11.6 nm/min compared to 18.8 nm/min). After the etching process, we immerse the substrate into boiling acetone with ultrasound agitation for 2 min, followed by cleaning in an O_2 plasma for 30 min. The plasma employs an O_2 flow rate of 45 sccm, coil and platen powers of 800 W and 50, respectively, and a chamber pressure of 35 mTorr. These steps result in vertical SiN_x light pipes with smoother and cleaner surfaces, as evidenced in Fig. 4(b). The light pipes have height/diameter aspect ratios of 2.13 and 8.2 for diameters of 4 μm and 0.9 μm, respectively. We then deposit SiO_2 by PECVD, whose highly conformal nature results in dome structures being formed over the light pipes, with radii approximately equal to the SiO_2 thickness (10 μm). This thickness (of 10 μm) refers to positions away from the light pipes. To obtain a cross sectional view that shows the light pipes underneath the domes, we use a focused ion beam (FIB) on a test sample. The results are shown in the SEM image of Fig. 4(c). We then use CMP to planarize the domes. In our CMP process, we glue the sample containing the SiN_x light pipes and SiO_2 domes to a metal holder using wax melted by heating to 160 °C. The metal holder weighs ~100 g. We then place the sample (with attached metal holder) face-down on a piece of lapping paper in a container filled with deionized (DI) water. The DI water acts as a lubricant. The lapping paper (3M Superabrasives and Microfinishing Systems Division; www.solutions.3m.com) comprises silicon carbide or aluminum oxide cylinders with diameters ~1–3 μm. The metal holder (to which the sample is attached) is moved over the lapping paper by hand in a sequence of eight different patterns in order to polish the sample surface uniformly. This process is repeated for 30 min, after which a decrease in dome height of ~8 μm is measured. The results are shown in the SEM of Fig. 4(d), in which an FIB is again used to produce a cross sectional view. For smaller light pipes (2 μm diameter), the polishing process can be seen to produce a final result that is more planar [Fig. 4(e)]. This is because for these pipes, the distance between the domes is larger and there is less SiO_2 to remove. In both cases [Figs. 4(d) and 4(e)], it can be seen that the domes have been largely polished away. Portions of the domes remain, but the surface is sufficiently flat so that it is possible to test the devices in a way that demonstrates the improved optical performance enabled by the light pipes. The results demonstrate the successful fabrication of silicon nitride light pipes embedded in silicon dioxide. In the next section, we demonstrate their integration with silicon photodetectors.

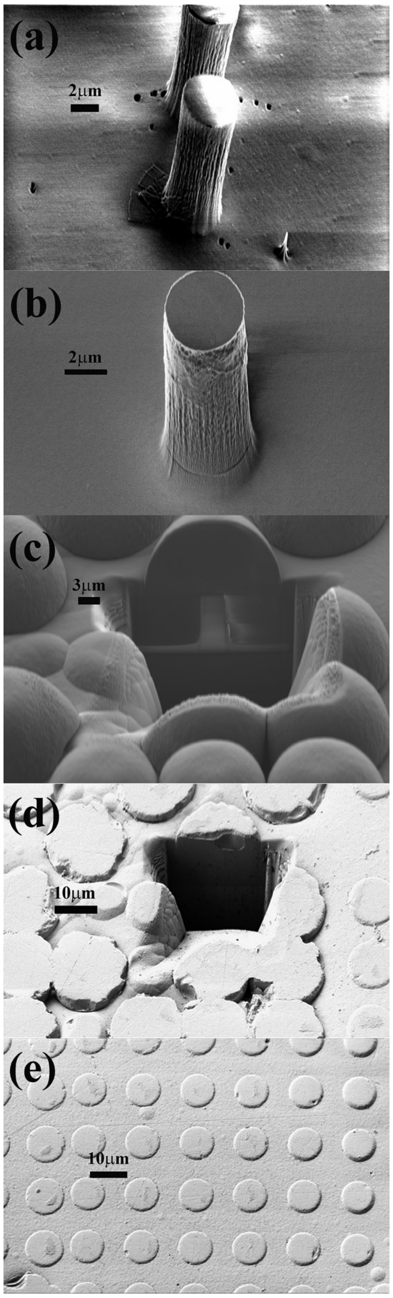

Fig. 4. (a) SEM image of SiN_x light pipes with heights of 8.5 μm. Dry etching is done in STS RIE system using an optimized recipe for vertical sidewalls and smooth side wall surfaces. Residual polymer can be seen at bottom of pipe. (b) SEM image of the SiN_x light pipes after removal of Al etch mask disks. Various methods for reducing the formation of polymer are applied (see text). (c) SEM image of sample upon which FIB milling has been employed to produce cross section showing light pipe after thick SiO_2 deposition. (d) SEM image after CMP process. Light pipe can also be seen in the cross sectional view (e) SEM image after CMP process is applied to a test sample having light pipes with smaller diameters (2 μm).

B. Photodetector fabrication and integration with silicon nitride light pipes

The photodiodes we report are lateral p-i-n structures. The starting substrate is an SOI wafer, with the [100] crystal orientation. The top layer is a 4 μm thick lightly p-type

Redistribution subject to AVS license or copyright; see http://scitation.aip.org/termsconditions. Download to IP: 202.120.43.250 On: Mon, 05 May 2014 11:30:58

doped silicon film with 1000 Ω-cm resistivity, with a 1 μm thick SiO_2 insulator layer on top of a 500 μm thick Si wafer. We begin by depositing silicon nitride to a thickness of 40 nm on the wafer to prevent oxidation and contamination. Alignment markers are defined by photolithography. Shipley 1813 photoresist with a thickness of ~1.3 μm is used. A resolution of ~1 μm is obtained by vacuum contact mode lithography (KarlSuss MJB3 or MJB4 mask aligners). The alignment markers are then etched into the substrate to a depth of ~4 μm by reactive ion etching (RIE) with CF_4 and Ar gases. We next form mesas, to isolate the photodiodes from one another electrically. This involves photolithography, this time using SU-8 resist (2002, ~2 μm thick) as the etch mask. We then etch to a depth 4.2 μm. The top silicon is therefore completely etched through to the SiO_2 insulating layer, ensuring electrical isolation of the photodiodes. We employ a release layer (Omnicoat from Micro Chem) with the SU-8 resist. This facilitates removal of the SU-8, which can otherwise be hard to achieve. The Omnicoat release layer and SU-8 are removed with an O_2 plasma. The wafer is then dipped into hydrofluoric acid (HF) to remove the oxide formed during the oxygen plasma process. We next produce the n+ type doped region of the photodiode. We first deposit a layer of silicon nitride to a thickness of 100 nm by PECVD. Lithography is then performed to define the region to be doped n+. Shipley S1813 resist is used (~1.3 μm thick) and baked after development at a temperature of 115 °C for 1 min. We then etch the silicon nitride film by reactive ion etching (Nexx RIE); the recipe is as follows: CF_4 flow rate is 15 sccm, Ar flow rate is 6 sccm, pressure is 10 mTorr, RF power is 100 W, and the microwave power is 306 W. The resultant SiN_x etch rate is 100 nm/min. In this step, the underlying silicon is also etched, to a depth of ~0.1 μm. We next dope the regions of the wafer in which openings in the silicon nitride have been formed. Spin-on-doping is used. A layer of phosphorosilica dopant is spun on to a silicon wafer, on which a silicon nitride film had been deposited. The wafer is baked at 200 °C for 15 min. We then place the samples to be doped on a plain silicon wafer. Pieces of silicon wafers are then added to this plain silicon wafer to act as spacers. We then place the wafer containing the doping material on top. This structure is then placed in a furnace (Lindberg) at 950 °C for 15 min. The furnace has nitrogen flow of 140 sccm and a forming gas flow of 300 sccm. The structure is then removed from the furnace. The top wafer, containing the doping material, is then removed, and the structure is returned to the furnace for annealing for a further 15 min. The samples are then placed in diluted HF (1:24 HF/water) to remove the phosphorosilicate glass formed on the silicon surface. A similar fabrication method is used to dope the p+ regions, with borosilica instead of phosphorosilica. A variety of photodiode structures are defined, with active region diameters ranging from 2 μm to 5 μm. The next step involves establishing the electrical connections to the photodiodes. We perform photolithography (Shipley S1813 resist), then thermally evaporate chrome and gold to thicknesses of 100 Å and 500 Å, respectively, with a deposition rate of 0.5 Å s^{-1}. The lift-off in acetone with ultrasonic agitation is performed for 1 min. The samples are then cleaned in acetone, methanol, and isopropanol, followed by a dehydration bake at 120 °C for 2 min. The samples are then annealed in a furnace (Lindberg) at 450 °C for 40 s to ensure that ohmic contacts to the Si are produced. This completes the fabrication of the silicon photodetectors. A microscope image of a typical device at this step is shown in Fig. 5(a). The active region width is 20 μm. The wide metal pads that connect to the n+ and p+ regions are 200 μm wide.

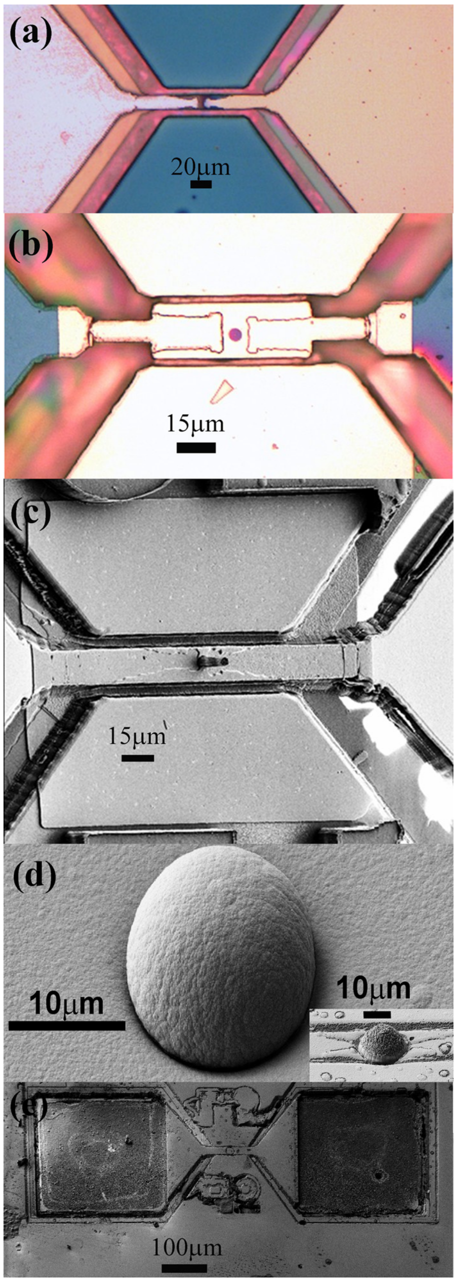

FIG. 5. (Color online) Photodiode fabrication. (a) Microscope image of complete lateral p-i-n Si-based photodiode (b) Microscope image of device after metal light blocking layer formation. (c) SEM image of SiN_x light pipe integrated with photodiode (d) SEM image of a test device which has only pipe after thick SiO_2 deposition and inset shows the real device after thick SiO_2 is deposited (e) SEM image after CMP process.

Redistribution subject to AVS license or copyright; see http://scitation.aip.org/termsconditions. Download to IP: 202.120.43.250 On: Mon, 05 May 2014 11:30:58

We now describe the fabrication of silicon nitride light pipes on the photodiodes. The process begins with the deposition of silicon nitride on the photodetectors to a thickness of 100 nm. This layer serves to electrically insulate the photodetectors from the metal layer we deposit next for light-blocking. It is therefore crucial that there be no pinholes in the silicon nitride film. The metal light-blocking layer serves to prevent light from being incident on the photodetector regions around the pillar, ensuring that the device has a photosensitive region with defined extent. The light-blocker layer is formed as follows. After the initial photolithography step, layers of chromium, aluminum, and chromium are evaporated to thicknesses of 20, 50, and 10 nm, respectively, followed by a lift-off process. The first Cr layer is for adhesion, while the second Cr layer serves to protect the Al when we later use a wet etchant (for Al) to remove the Al etch mask disks from the SiN_x light pipes. The resultant light-blocking layer appears as the bright region of Fig. 5(b). The opening in the light blocking layer, which represents the photosensitive region of the device, appears as a purple circle in Fig. 5(b). We next form the light pipes. Silicon nitride is deposited to a thickness of $\sim 8\,\mu$m step using the process described in Sec. II A. The deposition parameters that yielded the silicon nitride with optimized optical properties (Fig. 3 with SiH_4 flow rate of 35 sccm) are employed. We then define Al disks on the silicon nitride layer using photolithography, evaporation and lift-off. The disks are aligned with the active regions of the photodiodes. Light pipes are then produced by dry etching (ICP RIE), using the recipe described in Sec. II A. The light blocking metal layer also acts as an etch stop. The results are shown as Fig. 5(c). We next deposit SiO_2 (borophosphosilicate glass) by PECVD to a thickness of $\sim 9\,\mu$m. The results, obtained on a test device, are shown as Fig. 5(d). Photolithography is then performed to define the openings to be formed in the SiO_2 that enable electrical connections to the photodetectors. Here, an image reversal photoresist (AZ5214E photoresist, Clariant) is used in order to achieve a negative wall profile, as this is advantageous for the lift-of process. Thermal evaporation of aluminum, chromium, and titanium layers is then performed to thicknesses of 300, 100, and 100 nm, respectively. The lift-off process is then carried out. In the following RIE step, the flow rates of the C_4F_8 and SF_6 gases are both 10 sccm, the pressure is 7 mTorr, and coil and platen powers of 800 W and 100 W are used. The etching is performed for 40 min, resulting in an etch depth of 9.2 μm, as determined from a test sample. It can be seen from Fig. 5(d) inset that the SiO_2 surface is relatively rough. The metal mask thickness is not uniform and becomes completely etched through in some regions, including the SiO_2 domes, which then become rough due to micromasking. This is not a major source of concern, however, as the next step is planarization by CMP. This is motivated mainly to planarize the SiO_2 domes that form over each silicon nitride light pipe, but smoothes the other surfaces as well. The result is shown as Fig. 5(e). We then perform wire bonding, which completes the device. A schematic depiction of the final device is included as Fig. 6.

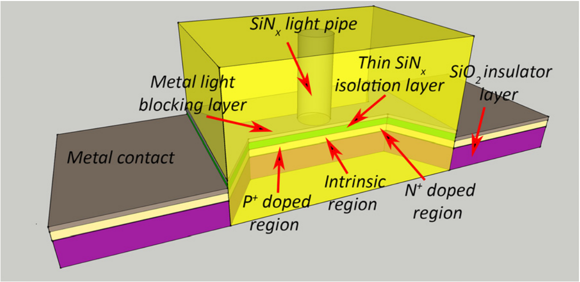

FIG. 6. (Color online) Schematic representation of completed device.

III. MEASUREMENTS

A. Current–voltage measurements

Upon the completion of the microfabrication of the lateral Si-based p-i-n photodiodes, we perform current–voltage (I-V) measurements upon them under dark and illuminated conditions. Illumination is provided with light from the tungsten lamp of a probe station microscope. Measurements are performed with a Keithley 2400 electrometer and Signatone microprobes. The measurement data are shown in Fig. 7. It can be seen that, for bias voltages close to 0 V, the ratio of photocurrent (with microscope lamp illumination) to dark current is four orders of magnitude (3×10^4). The dark current is on the order of a few picoamperes, while the photocurrent is on the order of tens of nanoamperes.

B. Scanning photocurrent measurements

We next describe the scanning photocurrent measurements employed to confirm the improved optical performance enabled by the light pipe structures.[5] Measurements are made both on devices containing light pipes, and on light pipe-free devices. Microscope images of the devices are shown in Figs. 8(a) and 8(b). We first place the devices on a probe station equipped with an electrometer (Keithley 2400) and measure the dark current to be $\sim 0.3\,\mu$A at a bias voltage of -0.2 V for both types of devices. We use this bias voltage in the scanning photocurrent measurements we perform

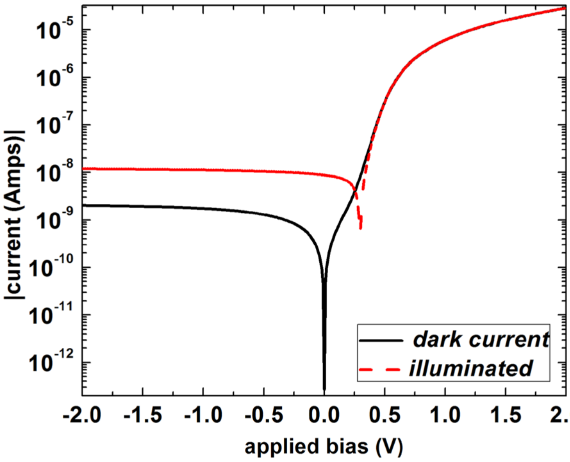

FIG. 7. (Color online) I-V characteristics of the fabricated Si based lateral p-i-n type photodetector. Photocurrent to dark current ratio at 0 V bias voltage is 4 orders of magnitude.

Redistribution subject to AVS license or copyright; see http://scitation.aip.org/termsconditions. Download to IP: 202.120.43.250 On: Mon, 05 May 2014 11:30:58

next. Each device is placed in a sample-scanning confocal microscope (WiTEC). In this system, fiber-coupled laser light ($\lambda = 532$ nm) is collimated, passed through a chopper, and focused by an objective lens (NA = 0.9, magnification = 100×) onto the device, which sits on a piezoelectric translation stage. The laser power from the objective lens is ~7 μW. The device is biased with an electrometer (Keithley 2400), and the current is measured with a lock-in amplifier. The reference signal is provided by the chopper, enabling the photocurrent to be extracted from the total current. The photocurrent is then recorded as a function of position as the device is scanned. Results obtained in this way are shown as Figs. 8(c) and 8(d) for the light pipe device and light pipe-free device, respectively. The bright circular spot of each image corresponds to the case where the focused laser beam is centered over the light pipe entrance. It should be noted that this data is obtained for the case where the laser spot is focused on the top surface. We observe that the photocurrent increases when the laser spot is centered over the mesa isolation trenches, but this does not reflect on the analysis of the light pipe properties. From Figs. 8(c) and 8(d), it can be seen that considerably higher photocurrent results from the light pipe device than the light pipe-free device. To explore this further, in Figs. 8(e) and 8(f) we plot the photocurrent as a function of distance for the devices with and without light pipes along the cross sections indicated in Figs. 8(c) and 8(d) (black lines). Figures 8(e) and 8(f) show that the peak photocurrent for the light pipe device is ~6.3 times larger than the peak value of the light pipe-free device. Interestingly, local minima appear in the centers of the photocurrent profiles for both the device containing the light pipe, and for the light-pipe free device. The cause of these minima is not fully understood. If we compare the photocurrent within these local minima, the ratio becomes ~4.2 times. We next consider the physical interpretation for the improvement enabled by the light pipe. Rather than full-field numerical electromagnetic modeling, we employ a ray-tracing model. While this is not as rigorous, it provides helpful physical insight. We note that our method is appropriate for the waveguides we study, as their diameters are significantly larger than the laser wavelength. For smaller waveguides, full-field simulations (e.g., Ref. 2) should be used. Full details of the method are provided in supplementary material document of Ref. 5, and only summarized here. We consider the light focused on the top surface of SiO_2 as consisting of a collection of rays with angles ranging from 0 to θ_{NA}, where $NA = \sin\theta_{NA}$ is the numerical aperture (=0.9) of the microscope objective. Ray tracing is then employed to determine the largest angle θ_{max} that a ray can be incident upon the top SiO_2 surface, and still be collected by the silicon photodetector, whose diameter ($R = 5$ μm) is defined by the opening in the Al light blocking layer. The light pipe device is regarded as comprising a 7 μm tall SiN_x cylinder (diameter 5 μm) encased in SiO_2 (8.7 μm thick). The light pipe-free device contains just the 8.7 μm thick SiO_2. The ray tracing predicts $\theta_{max} \approx 64°$ for the light-pipe device, while $\theta_{max} \approx 24°$ for the light-pipe free device. The photocurrents for the light pipe device, and the light pipe free device, are then predicted by integrating the intensities of the rays from 0 to θ_{max}, but with the reflection coefficients at the interface (air-SiO_2, SiO_2-SiN_x, SiO_2-Si, and SiN_x-Si) taken into account. For simplicity, these coefficients are found by averaging the Fresnel reflection coefficients for p- and s-polarizations. The results predict that a photocurrent for the light pipe device that is ~3.6 times larger than the light pipe-free device, in agreement with the experimentally measured trend.

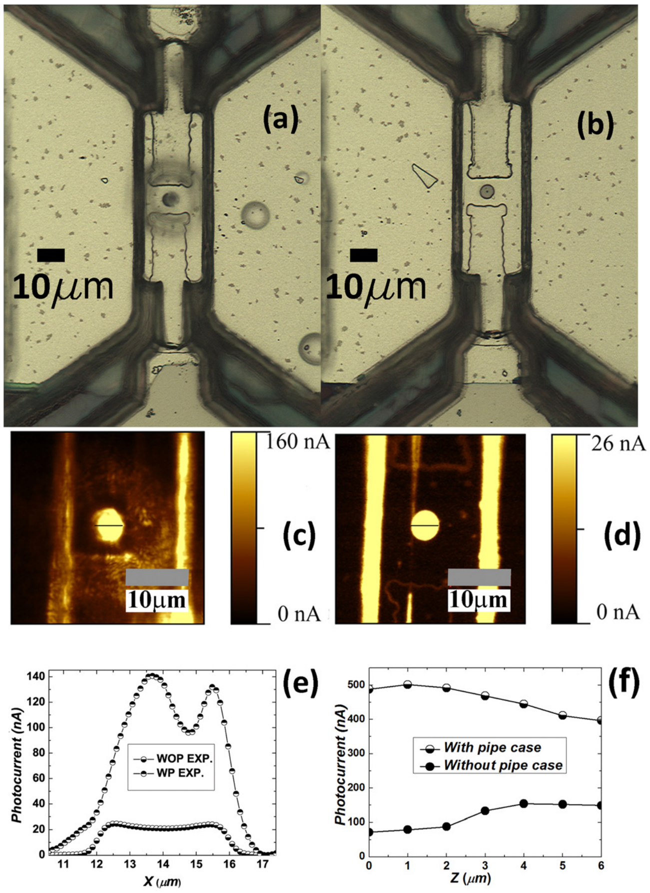

FIG. 8. (Color online) (a) Optical microscope image of completed device with light pipe. (b) Optical microscope image of light pipe free device fabricated for comparison purposes. Scanning photocurrent microscopy maps of (c) light pipe and (d) light pipe-free devices. (e) Photocurrent vs x-distance for light pipe ("experiment with light pipe") and light pipe-free ("experiment with out light pipe") devices measured along paths indicated in panels (c) and (d) with black lines. (f) Photocurrent vs vertical sample position (z), for another pair of light pipe and light pipe-free devices, measured under higher laser power.

To gain further insight into the improvement provided by the light pipes, we perform photocurrent measurements in which the device is scanned in the vertical (z) direction. The results are obtained by centering the laser spot over the light pipe, or over the photodetector for the light pipe free device, then measuring the photocurrent as the device is vertically translated by the piezoelectric stage over a distance of 6 μm. The results [Fig. 8(f)] show higher photocurrents than before due to the laser power being increased to 25 μW. In this figure, $z = 0$ μm corresponds to the laser spot being focused at the SiO_2 surface, while $z = 6$ μm corresponds to the device being moved by 6 μm so that the laser spot is within the device. It can be seen that, for the light pipe device, the photocurrent maximum is reached at $z \approx 1$ μm, due to the

Redistribution subject to AVS license or copyright; see http://scitation.aip.org/termsconditions. Download to IP: 202.120.43.250 On: Mon, 05 May 2014 11:30:58

coupling to the light pipe being largest when the laser beam is focused at its entrance. It then decreases as z increases, with the photocurrent being ∼1.3 times higher at $z = 0$ μm than $z = 6$ μm. This is consistent with the value predicted by the ray-tracing analysis (∼1.2 times). The photocurrent of the light pipe-free device increases ∼1.6 times as the position is varied from $z = 0$ μm to $z = 6$ μm, due to the waist being closer to the photodetector. This is again consistent with the trend predicted by ray-tracing of an increase of ∼2.3 times.

IV. CONCLUSION

In conclusion, we have demonstrated a fabrication method for vertical silicon nitride waveguides integrated with silicon photodetectors. We show that thick silicon nitride films with good optical transmission in the visible wavelength range can be achieved by optimization of the deposition conditions. We demonstrate that the silicon nitride pillars with near-vertical sidewalls can be achieved by fine tuning of the ratio between the flow rates of the etch gases. We also present that these silicon nitride pillars can be encased in SiO_2 by PECVD, followed by a simple CMP process. The final integration of the light pipes with silicon photodetectors is also described, by utilizing a new technique that enables the photosensitive region of the photodetectors to be well defined in its spatial extent. This involves the deposition of a light blocking layer (Al-Cr), with an opening defined in its center. To characterize the finished light pipe and light pipe-free devices, we perform current–-voltage and scanning photocurrent measurements. The latter clearly demonstrate the improvements enabled by the light pipes, and are found to be consistent with ray-tracing modeling. We therefore expect that the incorporation of light pipes into CMOS image sensors would result in significantly increased efficiency and reduced cross-talk.

ACKNOWLEDGMENTS

This work was supported by Zena Technologies and by Harvard University. Fabrication was performed in the Harvard Center for Nanoscale Systems (CNS), which was supported by the National Science Foundation. The authors thank Ling Xie, J. D. Deng, Yuan Lu, Steve Hickman, and David Lange for technical support and invaluable discussions.

[1] Y. Huo, C. C. Fesenmaier, and P. B. Catrysse, Opt. Express **18**, 5861 (2010).
[2] C. C. Fesenmaier, Y. Huo, and P. B. Catrysse, Opt. Express **16**, 20457 (2008).
[3] T. H. Hsu *et al.*, IEEE Electron Device Lett. **25**, 22 (2004).
[4] J. Gambino *et al.*, IEDM Int. Electron Devices Meet. **2006**, 1.
[5] T. Tut, Y. Dan, P. Duane, Y. Yu, M. Wober, and K. B. Crozier, Appl. Phys. Lett. **100**, 043504 (2012).
[6] W. N. Ye, P. Duane, M. Wober, and K. B. Crozier, J. Vac. Sci. Technol. B **29**, 031206 (2011).
[7] K. B. Crozier, D. A. Fletcher, G. S. Kino, and C. F. Quate, J. Microelectromech. Syst. **11**, 470 (2002).
[8] A. Gorin, A. Jaouad, E. Grondin, V. Aimez, and P. Charette, Opt. Express **16**, 13509 (2008).

Redistribution subject to AVS license or copyright; see http://scitation.aip.org/termsconditions. Download to IP: 202.120.43.250 On: Mon, 05 May 2014 11:30:58